Nitroaromatic compounds in six major Chinese cities: influence of different formation mechanisms on light absorption properties

Shasha Huang[1], Zhenxing Shen[1*], Xueting Yang[1], Gezi Bai[1], Leiming Zhang[2], Yaling Zeng[3], Jian Sun[1], Hongmei Xu[1], Steven Sai Hang Ho[4], Ying Zhang[5], Junji Cao[6]

[1]Department of Environmental Sciences and Engineering, Xi'an Jiaotong University, Xi'an, 710049, China

[2] Air Quality Research Division, Science and Technology Branch, Environment and Climate Change Canada, Toronto, Canada

[3] School of Environmental Science and Engineering, Southern University of Science and Technology, Shenzhen, 518055, China

[4]Divison of Atmospheric Sciences, Desert Research Institute, Reno, NV89512, United States

[5] Instruments Analysis Center of Xi'an Jiaotong University, Xi'an, 710049, China

[6] Institute of Atmospheric Physics, Chinese Academy of Sciences, Beijing, 100029, China

*Author to whom correspondence should be addressed. E-mail: zxshen@mail.xjtu.edu.cn (Zhenxing Shen)

Abstract

Nitroaromatic compounds (NACs) are important nitrogen organics in aerosol with strong light-absorbing and chemically reactive properties. In this study, NACs in six Chinese megacities, including Harbin (HB), Beijing (BJ), Xi'an (XA), Wuhan (WH), Chengdu (CD), and Guangzhou (GZ), were investigated for understanding their sources, gas-particle partitioning, and impact on BrC absorption properties. The concentrations of ΣNACs in $PM_{2.5}$ in the six cities ranged from 9.15 to 158.8 ng/m^3 in winter and from 2.02 to 9.39 ng/m^3 in summer. nitro catechols (NCs), nitro phenols (NPs), and nitro salicylic acids (NSAs) are the main components in ΣNACs, with NCs being dominant in particulate phase and NPs being dominant in the gas phase. Correlation analysis between different pollutant species revealed that coal and biomass combustions were the major sources of NACs in the northern cities during wintertime, while secondary formation dominated NACs in the southern cities during summertime. The contribution of ΣNACs to brown carbon (BrC) light absorption ranged from 0.85–7.98% during the wintertime and 2.07–6.44% during the summertime. The mass absorption efficiency at 365 nm (MAE_{365}) were highest for 4-nitrocatechol (4NC, 17.4–89.0 m^2/g), 4-methyl-5-nitrocatechol (4M5NC, 15.0–76.9 m^2/g), and 4-nitroguaiacol (4NG, 11.7–59.8 m^2/g). The formation of NCs and NG through oxidation and nitration of catechol and guaiacol led to a significant increase in aerosol light absorption. In contrast, NPs and NSAs formed by the photonitration and photooxidation in liquid phase showed high polarity but low light absorption ability, and the proportions of (NPs and NSAs) in the light absorption of ΣNACs were lower than 15.3% in the six megacities.

Keywords: NACs, Optical absorption, Source identification, Gas-particle phase partitioning, Spatial and Seasonal variation.

1. Introduction

Nitroaromatic compounds (NACs) are aromatic organics consisting of nitro and hydroxyl functional groups, which include nitro phenols and their derivatives (NPs),

nitro catechols and their derivatives (NCs), nitro salicylic acids (NSAs), nitro guaiacol (NG), etc (Chow et al., 2016; Kitanovski et al., 2012; Li et al., 2020c; Wang and Li, 2021). NACs are important light-absorbing contributors to brown carbon (BrC; Mohr et al., 2013; Teich et al., 2017; Xie et al., 2019; Yang et al., 2022). Although NACs only contribute 0.1–3.71% to $PM_{2.5}$ mass (Li et al., 2020c; Teich et al., 2017), these species contribute 4–50% or higher to BrC light absorption (Gu et al., 2022; Mohr et al., 2013). NACs could also produce genotoxic and pose cytotoxic effects on human health (Feng et al., 2022; Khan et al., 2022; Kovacic and Somanathan, 2014). NACs are unambiguous in the atmosphere and have been detected in cloud water (Desyaterik et al., 2013), rainwater (Schummer et al., 2009), fog (Richartz et al., 1990), snow (Vanni et al., 2001), and atmospheric particulate matter (PM; Song et al., 2021; Wang et al., 2018; Wang and Li, 2021).

NACs have been widely observed all over the world (SE Asia, Europe, US, etc.; Finewax et al., 2018; Frka et al., 2022; Kitanovski et al., 2021; Mayorga et al., 2021). NACs can be released from primary emissions from sources including biomass burning, coal combustion, vehicle exhaust, industrial emissions, etc (Lin et al., 2017; Lu et al., 2019a; Lu et al., 2019b; Lu et al., 2021). The emission factors of NACs from coal combustion are 0.2–10.1 mg/kg (Lu et al., 2019a). The content from industry emission, biomass burning, and vehicle exhaust are 0.1–0.3 $\mu g/m^3$, 2.0–99.5 $\mu g/m^3$, and 0.2–10.7 $\mu g/m^3$, respectively (Lu et al., 2019b; Lu et al., 2021; Wang et al., 2017). 4-nitrophenol (4NP) and its methyl derivatives are predominant in the emission of vehicles, leading to high total NACs concentrations ranging from 0.17–10.7 $\mu g/m^3$ (Lu et al., 2019b).

NACs can also be formed upon secondary liquid/gas phase oxidation of atmospheric precursors such as aromatic hydrocarbons (benzene, toluene, and xylene) and lignin pyrolysis products (phenol, m-cresol, guaiacol, catechol, and methyl catechol) (Kroflic et al., 2015; Mayorga et al., 2021; Salvador et al., 2021; Vidovic et al., 2019; Wang and Li, 2021; Wang et al., 2019; Yan et al., 2023; Yang et al., 2022). Nitrophenols (NPs) and 4-nitrocatechol (4NC) are formed by the oxidations of phenol or catechol initiated by hydroxyl (•OH) and nitrate ($\bullet NO_3$) radicals, respectively, in the presence of nitrogen dioxide (NO_2; Finewax et al., 2018). Methylnitrophenol (MNP) and

methylnitrocatechol are formed through photooxidation of m-cresol in the presence of nitrogen oxides (NO_x; Olariu et al., 2002). NPs, MNP, and 4NC are formed through gas-phase photooxidation of benzene and toluene in the presence of NO_x (Lin et al., 2015; Sato et al., 2007). The hydroxylation of nitrobenzene and the nitration or photoinitiation of phenols with the nitrating agents [e.g., nitric acid, nitrous acid, and chlorine nitrite ($ClNO_2$)] (Heal et al., 2007; Vione et al., 2003) also lead to elevated NAC concentration levels.

Due to the diversity of NACs and their sources and transformation pathways, most existing studies on NACs have focused on the production and transformation of a single NAC species or under a specific emission condition, resulting in incomplete knowledge of the NACs transformation pathways and associated environmental effects under different environmental conditions. To fill this knowledge gap covering a large scale across China, NACs contents in $PM_{2.5}$ (particles with aerodynamic diameter $\leq$ 2.5 μm) were measured in six representative cities. The objectives of this study include i) determining the spatiotemporal distributions of particle-phase NACs concentrations in the six Chinese megacities, ii) exploring the sources and transformation pathways of NACs, and iii) quantifying the contributions of NACs formed from different mechanisms to BrC light absorption.

2. Experiments and Methods

2.1. Sample collection

In this study, $PM_{2.5}$ samples were collected in urban areas in six megacities in China, including Harbin (HB; 45.75°N, 126.84°E), Beijing (BJ; 39.98°N, 116.36°E), Xi'an (XA; 34.22°N, 108.95°E), Wuhan (WH; 30.53°N, 114.39°E), Chengdu (CD; 30.69°N, 104.05°E), and Guangzhou (GZ; 23.15°N, 113.27°E), in December 2019 (winter) and July 2021 (summer). 10 samples were collected in each city in winter and summer for a total of 20 samples per city. These six cities represent the cultural and economic centers of Northeast, North, Northwest, Central, Southwest, and South China, respectively. The geographical latitudes of these cities span a wide range, which can well represent different climate zones and cover a variety of pollution scenarios. Such

a selection of sampling locations ensures the possibility of exploring characteristics of pollutants emissions and transformation pathways under different meteorological conditions. For example, winter heating (by burning coal and biomass) is popular in the northern cities (HB, BG, and XA) contributing to atmospheric $PM_{2.5}$ pollution. Southern cities (WH, CD, and GZ) have higher average temperature and humidity, which is conducive to liquid phase reaction and secondary generation of air pollutants.

24-h $PM_{2.5}$ samples were collected using a mini-volume sampler (AirMetrics, Springfield, OR, USA) at 5 L min^{-1} on 47 mm quartz fiber filters (Whatman, Maidstone, UK) in BJ, HB, and GZ; using a 100 L min^{-1} medium volume $PM_{2.5}$ sampler (HY-100SFB, Hengyuan, Qingdao, China) on a 90 mm quartz fiber filter (Whatman) in CD, and using a high volume sampler with a flow rate of 1.13 m^3 min^{-1} (HVS-$PM_{2.5}$ Tisch Environmental Inc., Cleves, OH, USA) on quartz fiber filters (203 mm × 254 mm, Whatman, QMA) in XA and WH. The quartz fiber filters for $PM_{2.5}$ collection were prebaked at 780 ℃ for 5 hours. After the sample collection, the filters were wrapped with clean aluminum foil and stored at -18 ℃. Detailed sampling procedures and information can be found in Sun et al (2022) and Zhang et al (2022c). Water-soluble inorganic ions (Na^+, NH_4^+, K^+, Mg^{2+}, Ca^{2+}, Cl^-, NO_3^-, and NO_2^-) were analyzed by ion chromatography (Dionex 500, Dionex Corp, USA).

2.2. Measurements of NACs in $PM_{2.5}$

10 nitroaromatic compounds in $PM_{2.5}$ were analyzed, including 4-nitrocatechol (4NC), 4-nitroguaiacol (4NG), 3-nitro-salicylic acid (3NSA), 5-nitrosalicylic acid (5NSA), 4-methyl-5-nitrocatechol (4M5NC), 4-nitrophenol (4NP), 3-methyl-4-nitrophenol (3M4NP), 2-methyl-4-nitrophenol (2M4NP), 4-methyl-2,6-dinitrophenol (MDNP), and 2,6-dimethyl-4-nitrophenol (DMNP), which are classified into four classes based on their function groups in molecules for further analysis, including nitro catechols (NCs=4NC and 4M5NC), nitrophenols (NPs=4NP, 3M4NP, 2M4NP, MDNP, and DMNP), nitrosalicylic acids (NSAs=3NSA and 5NSA), and nitroguaiacols (NG=4NG). The abbreviation of each target NAC is listed in Table S1.

A triple-quadrupole–MS system (TSQ Quantis, Thermo-Fisher, Agawam, MA, USA)

with an electrospray ionization source was applied to quantify NACs in the filter samples. Detailed methodology and instrumental settings are shown in Supporting Information (SI, Text S1). Briefly, each $PM_{2.5}$-loaded quartz filter sample was sonicated with 5 mL of methanol (HPLC, Macklin, Shanghai, China) for 30 min and passed through a 0.22-μm polytetrafluoroethylene syringe (WEGO, Weihai, Shandong, China) to remove residues. The filtrate was then dried under a gentle stream of high-purity nitrogen, redissolved with 50 μL of methanol, and subsequently injected into the analytical instrument. All target NACs were quantified by matching their retention times with authentic standards (> 97% purity; Shanghai Macklin Biochemical, Shanghai, China) and the characteristics of fragment ions under ionization. The relative standard deviation (RSD) of the concentration for each NAC was less than 15%. Following the method specified by the United States Environmental Protection Agency, the detection limit for each target species was calculated (Table S1). The recoveries of the NACs through the extraction were between 96.0~106.3%.

2.3 Optical property measurement

The light absorption of BrC in the ultraviolet-visible region [UV–Vis (i.e., 200 ~ 800 nm)] was measured using a USB2000 + UV–VIS–ES spectrometer, which is equipped with a 100-cm long liquid waveguide capillary cell (LWCC–3100, World Precision Instruments, Sarasota, FL, USA). The molecular structure of the ground state was optimized by selecting the B3LYP function basis set of 6-311g, with the Gaussian 09 software coupled with the time-deficit-density functional method. The excited state of each NAC was calculated, and the UV-visible spectra of the corresponding molecules were obtained. In the calculation, the solventization effect (solvent: methanol) was attenuated from the spectra. The optical parameters and the absorbance contributions of NACs were calculated and shown in Text S2.

2.4. Estimation of gas-phase NACs concentrations

The concentrations of gas-phase NACs were estimated from the measured particle-phase NACs content based on equilibrium absorption partitioning theory, as described

in the following equation (Barley and McFiggans, 2010; O'Meara et al., 2014; Pankow, 1994):

$$F_p = (1 + \frac{C^*}{C_{OA}})^{-1} = \frac{c_p}{c_g + c_p} \quad \text{(i)}$$

where F_p is the percentage of NACs in the particulate phase and C_{OA} is the concentration of organic aerosol (OA), calculated as 1.6 times of OA; C^* is the effective saturated mass concentration; and c_g and c_p are the contents of NACs in the gas- and particle-phases, respectively. C^* was calculated as below:

$$C^* = \frac{M10^6 \zeta P_V}{760RT} \quad \text{(ii)}$$

where M is the molar mass of NAC (g/mol); ζ is the activity coefficient of the substance (assumed to be 1); R is the gas constant (8.314 J(mol K)$^{-1}$); T is the temperature (K); and P_v (Pa) is the saturation pressure. P_v at average temperature was calculated using the online prediction tool for multiphase systems developed at the University of Manchester, UK (http://umansysprop.seaes.manchester.ac.uk/tool/vapour_pressure, UManSysProp) according to the method reported by Nannoolal et al (Joback and Reid, 1987; Nannoolal et al., 2008; Nannoolal et al., 2004). The aerosol liquid water content (ALWC) was estimated based on the mass concentrations of NH_4^+, SO_4^{2-}, NO_3^-, and Cl^- using the thermodynamic model in ISORROPIA-II (Liu et al., 2023; Shi et al., 2023).

3. Results and discussion

3.1 Seasonal and spatial distributions of NACs in $PM_{2.5}$

Table 1 summarizes the concentration levels of individual and total quantified NACs (ΣNACs) in $PM_{2.5}$ particles in the six megacities during the two seasons. The highest ΣNACs concentration during the winter was seen in HB (158.8 ± 68.6 ng/m^3), followed by XA (43.0 ± 16.3 ng/m^3), WH (31.0 ± 12.4 ng/m^3), GZ (19.4 ± 10.6 ng/m^3), BJ (10.8 ± 7.74 ng/m^3), and CD (9.15 ± 2.67 ng/m^3). A different ranking was observed during the summer, with the highest concentration in CD (9.39 ± 2.04 ng/m^3), followed by BJ (8.02 ± 0.30 ng/m^3), HB (7.18 ± 2.94 ng/m^3), GZ (3.97 ± 0.02 ng/m^3), XA (3.00 ± 0.02 ng/m^3), and WH (2.02 ± 0.03 ng/m^3). The levels of ΣNACs in winter were 1.35 to 22.1

times of those in summer in most cities, except in CD with winter level being 0.97 times of that in summer. The highest fraction of ΣNACs in $PM_{2.5}$ (ΣNACs/$PM_{2.5}$) was seen in HB (1.78‰), followed by XA (0.62‰), WH (0.40‰), GZ (0.38‰), BJ (0.36‰), and CD (0.09‰) in winter. The highest ΣNACs/$PM_{2.5}$ was in BJ (0.64‰), followed by CD (0.25‰), HB (0.23‰), GZ (0.15‰), XA (0.09‰), and WH (0.09‰) in summer. The seasonal pattern with higher ΣNACs/$PM_{2.5}$ in winter than summer was consistent with those reported in Shanghai (Cai et al., 2022), Hong Kong (Chow et al., 2016), Jinan (Li et al., 2020b; Wang et al., 2018), and Beijing (Ren et al., 2022; Yang et al., 2020).

NCs, NPs, NSAs, and NG contributed 37.9–77.7%, 9.42–40.7%, 4.51–25.5%, and 0.16–4.89%, respectively, to ΣNACs in winter (Fig 1b), and 4.95–44.5%, 10.2–59.9%, 20.4–58.8%, and 0.70–14.8%, respectively, in summer (Fig. 1c). The NSAs/ΣNACs in HB, XA, WH, and CD were lower in winter than summer (4.51 vs 31.54%, 8.67 vs 58.83%, 13.84 vs 51.90%, and 12.72 vs 42.46%, respectively). The fractions of NPs in HB, BJ, and CD were higher in summer than winter, but the opposite trend was seen in XA, WH, and GZ. In BJ, the fraction of NPs in ΣNACs were the highest in both seasons, indicating their relatively stable sources. NG had the lowest fraction in ΣNACs in winter in all megacities except HB, but also showed higher fractions in HB, BJ, and CD during the summertime.

Insert table 1

Insert figure 1

3.2 Source identification of NACs

The sources and formation pathways of NACs in the six megacities were identified by correlation analysis between ΣNACs and other tracers (Fig. 2). In winter, ΣNACs significantly correlated with K^+ and SO_4^{2-}, which are typical tracers for biomass and coal combustion sources, respectively, in all the cities except WH. Thus, biomass burning and coal combustion sources contributed significantly to NACs in northern and southern cities during the wintertime, as has been reported in earlier studies (Huang et al., 2023; Salvador et al., 2021; Wang et al., 2017). The correlation between NCs and

NPs was significant (Pearson correlation analysis, P<0.05), especially in XA, CD and GZ (Table S3), indicating that the primary and precursor sources of the two classes of NACs are similar. The variation in the relationship between ΣNACs and NO_3^- suggests that there are secondary sources of NACs in winter in these cities. NO_3^- correlated well with NSAs in the northern cities, and with NCs, NPs, and NSAs in BJ, XA, CD, and GZ. The correlations of NSAs with NCs and NPs were also prominent, especially in GZ and XA, which indicates that the sources of NCs, NPs, and NSAs in winter are similar in the same city. It also indicates that secondary reactions are one of the sources of NACs in the cities mentioned above in winter. However, there was no correlation between NG and other NACs, suggesting unique formation pathway of NG.

In summer, the correlation between ΣNACs and K^+ was not as significant as that in winter, suggesting a reduced contribution from biomass burning. The correlations among the NACs species were also significantly weaker than those in winter, suggesting more diversified formation pathways of the NACs in summer. The strong correlations between NPs (DMNP with 3MNP, 2MNP, and 4NP) indicate that the origin and chemical transformation of NACs of the same class were similar. The correlation between NSAs and NCs in HB, BJ, XA, and GZ were significant (P<0.05). NCs and NSAs positively correlated with O_3 (NCs-O_3: R = 0.563, P<0.05; NSAs-O_3: R = 0.346, P<0.05), but NG negatively correlated with O_3 (R = -0.783) in XA. The photolysis of O_3 is the main source of •OH. The photo-oxidation and subsequent nitration of the precursors such as benzene and toluene could both produce NACs (Mayorga et al., 2021; Wang and Li, 2021; Yang et al., 2022). Moreover, precursor oxidation initiated by •OH and •NO_3 could occur during the day- and nighttime (Li et al., 2020a). NCs (R=0.706, P<0.05), NPs (R=0.718, P<0.05), and NSAs (R=0.801, P<0.01) significantly correlated with NO_3^- in HB. Among the southern cities, NSAs significantly correlated with NO_3^- in WH (R=0.791, P<0.05) and CD (R=0.677, P<0.05), while 5NSA significantly correlated with NO_2^- in GZ (R=0.702, P<0.05). The presence of nitrate promotes the formation of gaseous nitrite and nitrogenous aromatic compounds in the atmosphere (Deng et al., 2021). These results suggest the importance of secondary formation in the production of NACs in summer, especially in southern cities.

The above discussions suggested very different pollution sources of NACs between winter and summer. Overall, NACs in the six megacities were mainly derived from biomass and coal combustion in winter. NCs, NPs, and NSAs in BJ, XA, CD, and GZ could also be from secondary formation in winter. On the contrary, NACs were mainly from secondary formation in summer, as further illustrated below. The main source of oxidants for NACs formation in XA was •OH produced by O_3, while the formation of NCs, NPs, and NSAs in HB and NSAs in the southern cities was mainly from the oxidation of nitrogen-containing radicals.

Insert figure 2

3.3 The formation of NACs

The different sources and formation mechanisms between different NACs species and subsequent complex atmospheric chemistry processes resulted in varying NACs levels in each megacity. In the discussion below, the calculated *Fp* and ALWC of NACs and the correlation analysis results were used together to explore the possible formation mechanisms of NACs in atmospheric aerosols in the studied cities.

In winter, the concentrations of ∑NACs were higher in northern than southern cities due to extensive coal and biomass combustion for winter heating in most northern cities (Huang et al., 2023; Zhang et al., 2022b). In BJ, NACs emissions from direct sources were lower, but NACs formation from secondary sources were higher compared to the other northern cities due to the stricter emission reduction measures implemented in this city, such as the one for switching coal to gas (Yuan et al., 2023). The 4NC significantly and positively correlated with ALWC in HB (Fig. S2a), indicating secondary production in the liquid phase of 4NC in winter in this city. Earlier studies suggested that NPs was mainly from vehicle and industrial emissions (Lu et al., 2019a; Yang et al., 2020). However, the significant positive correlations between 4NPs and ALWC in winter in GZ and BJ indicated that a significant amount of NPs was generated from secondary production.

NSAs correlated relatively well with K^+, NO_2, and O_3 in both southern and northern cities, implying that NSAs were associated with both primary and secondary sources. Figure S2 shows significant positive correlations between NSAs and ALWC in HB, BJ, and GZ during wintertime, suggesting the occurrence of secondary production of NSAs in the liquid phase. The phenolic substances in the particle phase are activated into phenoxy radicals by the hydrogen extraction of •OH, which are subsequently nitrated by $•NO_3$ to form 3NSA and 5NSA (Fig. 3; Jang and Kamens, 2001; Shi et al., 2023). Note that these phenols are mainly derived from pyrolysis of lignin during biomass combustion in winter (Iinuma et al., 2010). NSAs are mainly from secondary oxidative nitration of precursors from biomass combustion in winter. The high O_3 levels in HB, GZ, and WH ensured rich oxidants for the oxidation of precursors, and high NO_2 levels in winter in all of the six cities provided enough NO_3^- for nitration, which led to the high contents of NSAs in winter in HB, GZ and WH.

NG significantly positively correlated with NO_2^- in HB (P<0.01) because their common linkage with $•NO_3$. It is known that NO_2^- can produce $•NO_3$ (Kroflic et al., 2021; Yang et al., 2021). NG is produced from the oxidation and nitration of guaiacol released from biomass combustion emissions (Cai et al., 2022). Therefore, the nitration of $•NO_3$ with rich guaiacol released from biomass combustion in winter in HB led to the highest NG content in HB among the six megacities.

In summer, NACs were significantly reduced due to reduced biomass combustion sources. Most of the precursors for the secondary production of NACs were derived from VOCs in summer because the high levels of VOCs and sufficient O_3 (Table. S4) are conducive to the formation of NACs. The main sources of NCs (biomass and coal combustion) decreased in summer compared to winter, resulting in significantly lower levels of NCs in summer. The direct sources of NPs (industry and vehicle emissions) were relatively stable in summer. NSAs and NGs were primarily from secondary reactions, and their proportions in NACs increased significantly in summer compared to the cases in winter.

During summertime, significant correlations between 3NSAs, NPs and ALWC were

only observed in WH, suggesting that most of NACs in the six megacities were mainly derived from the oxidation of •OH and $•NO_3$ in the gas phase. According to Figure 2, biomass burning in HB resulted in higher ∑NACs content compare to XA, WH, and GZ. CD is located in the Sichuan Basin, which is not conducive to the diffusion of air pollutants because of its unique topography, static wind, and high humidity (Zhang et al., 2022a; Zhao et al., 2018). As a result, the residence times of VOCs and other precursors in the atmosphere increase, and thus enhance the secondary generation of NACs, resulting in the highest ∑NACs in CD among the southern cities in summer.

Discussions presented above focused only on particle-phase NACs. It should be noted that gas-particle partitioning of NACs also have significant impacts on the contents of NACs in $PM_{2.5}$ (Fig. S3). The large *Fp* values of NCs in winter (27.9-99.4%) indicate that these species mainly distributed in the particle phase, especially in the northern megacities. The much lower *Fp* of the NPs than the other three types of NACs indicated NPs being mostly in the gas phase, which also partly explained the higher levels of NCs than NPs in $PM_{2.5}$. The close to 1 value of *Fp* of NSAs suggested that NSAs were entirely distributed in the particle phase, despite that these species could also be formed through secondary production in the gas phase in summer. Moreover, *Fp* values were smaller in summer than winter for every species of NACs at any of the sites, consistent with the seasonal patterns of ∑NACs levels.

Insert figure 3

3.4 The influence of NACs formation on their light absorption

NACs are important BrC chromophores (Frka et al., 2022; Xie et al., 2017; Yang et al., 2022). The contributions of ΣNACs and the four subclasses to the total light absorption of the BrC at the wavelength of 365 nm were determined with the Gaussian software (Fig. 4). During the wintertime, the contribution of ΣNACs to the total light absorption of BrC ($\sum_{NAC/BrC\_absorption}$) was the highest in XA (7.98%), followed by GZ (7.89%), HB (7.11%), WH (4.18%), CD (1.74%), and lowest in BJ (0.85%), while during the summertime the highest was in GZ (6.44%), followed by WH (3.00%), XA

(2.66%), HB (2.51%), CD (2.26%), and lowest in BJ (2.07%). It should be noted that the light absorption contributions of NACs were generally higher in winter than summer (Li et al., 2020d; Yuan et al.,2021). Figure S4 shows the atomic absorption coefficient profiles of the ten NACs considered in this study, from which we can conclude that NCs and NG are strong light-absorbing species while NPs and NSAs are weak light-absorbing species. For example, 4NC, 4M5NC, and 4NG have prominent absorption properties at 365 nm, with their MAE_{365} being 17.35–88.99, 14.98–76.85, and 11.66–59.82 m^2/g, respectively (Table. S5). In contrast, 4NP, 3NSA, and 5NSA have much weaker absorption properties with their MAE_{365} being only 0.00–0.05, 0.47–2.43, 0.00–0.31 m^2/g, respectively.

Insert figure 4

During the wintertime, NCs contributed most to the light absorption of ΣNACs, accounting for >80% in all of the six megacities (Fig. 5). NG and NPs contributed appreciable fractions, accounting for 0.18–10.43% and 0.86–6.68%, respectively. NSAs contributed minimum fractions, only 0.07–0.40%. Biomass and coal combustion were the main sources of NCs in winter, and there was a high correlation between the mass fraction of NCs and the light absorption of BrC (R = 0.804, P < 0.05). Thus, a large number of primary emission sources from biomass and coal combustion in winter resulted in a strong light-absorbing contribution from NCs.

During the summertime, the contributions of the four subclasses in ΣNACs to the light absorption of ΣNACs in descending order were NCs (20.76–94.82%) > NG (1.81–63.91%) > NPs (0.86–14.56%) > NSAs (0.77–1.95%). In summer, most NACs were formed from secondary reactions of VOCs precursors under high ambient temperature condition and oxidants levels. 4NC and 4NG are from the precursors replaced by nitration of NO_2 after oxidation of •OH and $•NO_3$ (Fig. 3). Their strong light-absorbing properties indicate that the oxidation-nitration process of catechol and guaiacol led to a significant increase in aerosol light absorption. Yang et al. observed a greater increase in light absorption during nitrate-mediated photo-oxidation of guaiacol (Yang et al.,

2021). The phenomenon in our study suggests that the presence of nitro groups on phenolic compounds is important for the enhancement of light absorption of BrC. The NCs and NG formed by the precursors of nitration substitution could enhance the light absorption capacity of BrC. NPs were formed by photonitration of precursors such as phenol under UV nitrite irradiation or by hydroxylation and nitration of benzene in the presence of nitrite/nitrous acid (NO_2^-/HNO_2) in aqueous solution (Vione et al., 2004; Vione et al., 2001). Salicylic acid and other phenols were activated by hydrogen extraction of •OH and nitrate of •NO_3 to form NSAs (Shi et al., 2023). Among the four subclasses of NACs, the mass fraction of NSAs in ΣNACs ranked the third, but its light absorption contribution to ΣNACs ranked the lowest in all of the six megacities. Moreover, the mass contribution of NPs to ΣNACs were 3.87–14.4 times of its light absorption contribution. These indicate that NPs and NSAs formed from liquid phase photonitration or photooxidation cannot enhance the light absorption of BrC.

Insert figure 5

4. Conclusions

This study determined the NACs in six megacities in China during one summer and one winter month. Typically, the higher contents of ΣNACs and higher NCs fractions in ΣNAC in winter than summer resulted in higher contributions of ΣNACs to the absorbance of BrC in winter in the six megacities. Coal and biomass combustion were the major sources of NACs during wintertime, particularly in northern cities. Secondary formation accounts for a higher proportion of NACs in southern than northern cities in summer. NSAs were mainly formed in liquid-phase secondary reactions, while NCs were released from primary emissions of biomass and coal combustion, and these two groups of chemical species mainly distributed in the particle phase. NPs were the main component of the gas-phase NACs and were from secondary generation and vehicle emissions. NCs and NG were strong light-absorbing species while NPs and NSAs were weak light-absorbing species. The oxidation-nitration process of catechol and guaiacol led to a significant increase in aerosol light absorption, and the liquid-phase

photoionization and photo-oxidation for the formation of NPs and NSAs showed weak light absorption of BrC. Future studies should include more intermediate chemical species involved in the NACs formation processes to advance our understanding on the detailed transformation mechanisms under different atmospheric conditions.

Acknowledgments

This research was financially supported by the Key R & D project of Shaanxi Province (2022ZDLSF06-07) and the State Key Laboratory of Loess and Quaternary Geology, Institute of Earth Environment, CAS (SKLLQG2103).

References

Barley, M. H., and McFiggans, G., 2010. The critical assessment of vapour pressure estimation methods for use in modelling the formation of atmospheric organic aerosol. Atmos. Chem. Phys. 10(2), 749-767.

Cai, D. M.; Wang, X. K.; George, C.; Cheng, T. T.; Herrmann, H.; Li, X.; Chen, J. M., 2022. Formation of secondary nitroaromatic compounds in polluted urban environments. J. Geophys. Res.-Atmos. 127(10).

Chow, K. S.; Huang, X. H. H.; Yu, J. Z., 2016. Quantification of nitroaromatic compounds in atmospheric fine particulate matter in Hong Kong over 3 years: field measurement evidence for secondary formation derived from biomass burning emissions. Environmental Chemistry. 13(4), 665-673.

Deng, H. F.; Liu, J. P.; Wang, Y. Q.; Song, W.; Wang, X. M.; Li, X.; Vione, D.; Gligorovski, S., 2021. Effect of inorganic salts on N-containing organic compounds formed by heterogeneous reaction of NO_2 with oleic acid. Environmental Science & Technology. 55(12), 7831-7840.

Desyaterik, Y.; Sun, Y.; Shen, X.; Lee, T.; Wang, X.; Wang, T.; Collett, J. L., Jr., 2013. Speciation of "brown" carbon in cloud water impacted by agricultural biomass burning in eastern China. J. Geophys. Res.-Atmos. 118(13), 7389-7399.

Feng, R.; Xu, H. M.; Gu, Y. X.; Wang, Z. X.; Han, B.; Sun, J.; Liu, S. X.; Lu, H. W.; Ho, S. S. H.; Shen, Z. X.; Cao, J. J., 2022. Variations of personal exposure to particulate nitrated phenols from heating energy renovation in China: The first assessment on associated toxicological

impacts with particle size distributions. Environmental science & technology. 56(7), 3974-3983.

Finewax, Z.; de Gouw, J. A.; Ziemann, P. J., 2018. Identification and quantification of 4-Nitrocatechol formed from OH and NO_3 radical-initiated reactions of catechol in air in the presence of NO_x: Implications for secondary organic aerosol formation from biomass burning. Environmental Science & Technology. 52(4), 1981-1989.

Frka, S.; Sala, M.; Brodnik, H.; Stefane, B.; Kroflic, A.; Grgic, I., 2022. Seasonal variability of nitroaromatic compounds in ambient aerosols: Mass size distribution, possible sources and contribution to water-soluble brown carbon light absorption. Chemosphere. 299, 134381.

Gu, C. J.; Cui, S. J.; Ge, X. L.; Wang, Z. Y.; Chen, M. J.; Qian, Z. H.; Liu, Z. Y.; Wang, X. F.; Zhang, Y. J., 2022. Chemical composition, sources and optical properties of nitrated aromatic compounds in fine particulate matter during winter foggy days in Nanjing, China. Environmental Research. 212.

Heal, M. R.; Harrison, M. A. J.; Cape, J. N., 2007. Aqueous-phase nitration of phenol by N_2O_5 and $ClNO_2$. Atmos. Environ. 41(17), 3515-3520.

Huang, S. S.; Yang, X. T.; Xu, H. M.; Zeng, Y. L.; Li, D.; Sun, J.; Ho, S. S. H.; Zhang, Y.; Cao, J. J.; Shen, Z. X., 2023. Insights into the nitroaromatic compounds, formation, and light absorption contributing emissions from various geological maturity coals. Sci. Total Environ. 870.

Iinuma, Y.; Böge, O.; Gräfe, R.; Herrmann, H., 2010. Methyl-nitrocatechols: atmospheric tracer compounds for biomass burning secondary organic aerosols. Environmental Science & Technology. 44(22), 8453-8459.

Jang, M. S.; Kamens, R. M., 2001. Characterization of secondary aerosol from the photooxidation of toluene in the presence of NO_x and 1-propene. Environmental Science & Technology. 35(18), 3626-3639.

Joback, K. G.; Reid, R. C., 1987. Estimation of pure-component properties from group-contributions. Chemical Engineering Communications. 57(1-6), 233-243.

Khan, F.; Jaoui, M.; Rudzinski, K.; Kwapiszewska, K.; Martinez-Romero, A.; Gil-Casanova, D.; Lewandowski, M.; Kleindienst, T. E.; Offenberg, J. H.; Krug, J. D.; Surratt, J. D., 2022. Cytotoxicity and oxidative stress induced by atmospheric mono-nitrophenols in human lung cells. Environ. Pollut. 301.

Kitanovski, Z., Hovorka, J., Kuta, J., Leoni, C., Prokes, R., Sanka, O., Shahpoury, P., Lammel, G., 2021. Nitrated monoaromatic hydrocarbons (nitrophenols, nitrocatechols, nitrosalicylic acids) in ambient air: levels, mass size distributions and inhalation bioaccessibility. Environ. Sci. Pollut. Res. 28, 59131-59140.

Kitanovski, Z., Shahpoury, P., Samara, C., Voliotis, A., Lammel, G., 2020. Composition and mass size distribution of nitrated and oxygenated aromatic compounds in ambient particulate matter from southern and central Europe-implications for the origin. Atmos. Chem. Phys. 20, 2471-2487.

Kitanovski, Z.; Grgic, I.; Vermeylen, R.; Claeys, M.; Maenhaut, W., 2012. Liquid chromatography tandem mass spectrometry method for characterization of monoaromatic nitro-compounds in atmospheric particulate matter. Journal Of Chromatography A. 1268, 35-43.

Kovacic, P.; Somanathan, R., 2014. Nitroaromatic compounds: Environmental toxicity, carcinogenicity, mutagenicity, therapy and mechanism. Journal Of Applied Toxicology. 34(8), 810-824.

Kroflic, A., Anders, J., Drventic, I., Mettke, P., Boge, O., Mutzel, A., Kleffmann, J. and Herrmann, H., 2021. Guaiacol nitration in a simulated atmospheric aerosol with an emphasis on atmospheric nitrophenol formation mechanisms. Acs Earth And Space Chemistry. 5(5), 1083-1093.

Kroflic, A.; Grilc, M.; Grgic, I., 2015. Unraveling pathways of guaiacol nitration in atmospheric waters: Nitrite, a source of reactive nitronium ion in the atmosphere. Environmental Science & Technology. 49(15), 9150-9158.

Li, C. L.; He, Q. F.; Hettiyadura, A. P. S.; Kafer, U.; Shmul, G.; Meidan, D.; Zimmermann, R.; Brown, S. S.; George, C.; Laskin, A.; Rudich, Y., 2020a. Formation of secondary brown carbon in biomass burning aerosol proxies through NO_3 radical reactions. Environmental Science & Technology. 54(3), 1395-1405.

Li, M.; Wang, X. F.; Lu, C. Y.; Li, R.; Zhang, J.; Dong, S. W.; Yang, L. X.; Xue, L. K.; Chen, J. M.; Wang, W. X., 2020b. Nitrated phenols and the phenolic precursors in the atmosphere in urban Jinan, China. Sci. Total Environ. 714.

Li, X.; Wang, Y. J.; Hu, M.; Tan, T. Y.; Li, M. R.; Wu, Z. J.; Chen, S. Y.; Tang, X. Y., 2020c. Characterizing chemical composition and light absorption of nitroaromatic compounds in the

winter of Beijing. Atmos. Environ. 237.

Li, X., Yang, Y., Liu, S., Zhao, Q., Wang, G., Wang, Y., 2020d. Light absorption properties of brown carbon (BrC) in autumn and winter in Beijing: Composition, formation and contribution of nitrated aromatic compounds. Atmos. Environ. 223.

Lin, P.; Bluvshtein, N.; Rudich, Y.; Nizkorodov, S. A.; Laskin, J.; Laskin, A., 2017. Molecular chemistry of atmospheric brown carbon inferred from a nationwide biomass burning event. Environmental Science & Technology. 51(20), 11561-11570.

Lin, P.; Liu, J.; Shilling, J. E.; Kathmann, S. M.; Laskin, J.; Laskin, A., 2015. Molecular characterization of brown carbon (BrC) chromophores in secondary organic aerosol generated from photo-oxidation of toluene. Physical Chemistry Chemical Physics. 17(36), 23312-23325.

Liu, T.; Xu, Y.; Sun, Q. B.; Xiao, H. W.; Zhu, R. G.; Li, C. X.; Li, Z. Y.; Zhang, K. Q.; Sun, C. X.; Xiao, H. Y., 2023. Characteristics, origins, and atmospheric processes of amines in fine aerosol particles in winter in China. J. Geophys. Res.-Atmos. 128(14).

Lu, C.; Wang, X.; Li, R.; Gu, R.; Zhang, Y.; Li, W.; Gao, R.; Chen, B.; Xue, L.; Wang, W., 2019a. Emissions of fine particulate nitrated phenols from residential coal combustion in China. Atmos. Environ. 203, 10-17.

Lu, C. Y.; Wang, X. F.; Dong, S. W.; Zhang, J.; Li, J.; Zhao, Y. A.; Liang, Y. H.; Xue, L. K.; Xie, H. J.; Zhang, Q. Z.; Wang, W. X., 2019b. Emissions of fine particulate nitrated phenols from various on-road vehicles in China. Environmental Research. 179.

Lu, C. Y.; Wang, X. F.; Zhang, J.; Liu, Z. Y.; Liang, Y. H.; Dong, S. W.; Li, M.; Chen, J.; Chen, H. B.; Xie, H. J.; Xue, L. K.; Wang, W. X., 2021. Substantial emissions of nitrated aromatic compounds in the particle and gas phases in the waste gases from eight industries. Environ. Pollut. 283.

Mayorga, R. J.; Zhao, Z.; Zhang, H., 2021. Formation of secondary organic aerosol from nitrate radical oxidation of phenolic VOCs: Implications for nitration mechanisms and brown carbon formation. Atmos. Environ. 244.

Mohr, C.; Lopez-Hilfiker, F. D.; Zotter, P.; Prevot, A. S. H.; Xu, L.; Ng, N. L.; Herndon, S. C.; Williams, L. R.; Franklin, J. P.; Zahniser, M. S.; Worsnop, D. R.; Knighton, W. B.; Aiken, A. C.; Gorkowski, K. J.; Dubey, M. K.; Allan, J. D.; Thornton, J. A., 2013. Contribution of nitrated phenols to wood burning brown carbon light absorption in detling, United Kingdom during

winter time. Environmental Science & Technology. 47(12), 6316-6324.

Nannoolal, Y.; Rarey, J.; Ramjugernath, D., 2008. Estimation of pure component properties-Part 3. Estimation of the vapor pressure of non-electrolyte organic compounds via group contributions and group interactions. Fluid Phase Equilib. 269(1-2), 117-133.

Nannoolal, Y.; Rarey, J.; Ramjugernath, D.; Cordes, W., 2004. Estimation of pure component properties Part 1. Estimation of the normal boiling point of non-electrolyte organic compounds via group contributions and group interactions. Fluid Phase Equilib. 226, 45-63.

O'Meara, S., Booth, A. M.; Barley, M. H.; Topping, D.; McFiggans, G., 2014. An assessment of vapour pressure estimation methods. Physical Chemistry Chemical Physics. 16(36), 19453-19469.

Olariu, R. I.; Klotz, B.; Barnes, I.; Becker, K. H.; Mocanu, R., 2002. FT-IR study of the ring-retaining products from the reaction of OH radicals with phenol, o-, m-, and p-cresol. Atmos. Environ. 36(22), 3685-3697.

Pankow, J. F., 1994. An absorption-model of the gas aerosol partitioning involved in the formation of secondaty organic aerosol. Atmos. Environ. 28(2), 189-193.

Ren, Y.; Wei, J.; Wang, G.; Wu, Z.; Ji, Y.; Li, H., 2022. Evolution of aerosol chemistry in Beijing under strong influence of anthropogenic pollutants: Composition, sources, and secondary formation of fine particulate nitrated aromatic compounds. Environmental Research. 204.

Richartz, H.; Reischl, A.; Trautner, F.; Hutzinger, O., 1990. Nitrates phenols in fog. Atmospheric Environment Part a-General Topics. 24(12), 3067-3071.

Salvador, C. M. G.; Tang, R. Z.; Priestley, M.; Li, L. J.; Tsiligiannis, E.; Le Breton, M.; Zhu, W. F.; Zeng, L. M.; Wang, H.; Yu, Y.; Hu, M.; Guo, S.; Hallquist, M., 2021. Ambient nitro-aromatic compounds-biomass burning versus secondary formation in rural China. Atmos. Chem. Phys. 21(3), 1389-1406.

Sato, K.; Hatakeyama, S.; Imamura, T., 2007. Secondary organic aerosol formation during the photooxidation of toluene: NO_x dependence of chemical composition. Journal Of Physical Chemistry A. 111(39), 9796-9808.

Schummer, C.; Groff, C.; Al Chami, J.; Jaber, F.; Millet, M., 2009. Analysis of phenols and nitrophenols in rainwater collected simultaneously on an urban and rural site in east of France. Sci. Total Environ. 407(21), 5637-5643.

554 Shi, X. D.; Qiu, X. H.; Li, A. L.; Jiang, X.; Wei, G. Y.; Zheng, Y.; Chen, Q.; Chen, S. Y.; Hu, M.;
555 Rudich, Y.; Zhu, T., 2023. Polar nitrated aromatic compounds in urban fine particulate matter:
556 A focus on formation via an aqueous-phase radical mechanism. Environmental Science &
557 Technology. 57(13), 5160-5168.
558 Song, K.; Guo, S.; Wang, H.; Yu, Y.; Wang, H.; Tang, R.; Xia, S.; Gong, Y.; Wan, Z.; Lv, D.; Tan,
559 R.; Zhu, W.; Shen, R.; Li, X.; Yu, X.; Chen, S.; Zeng, L.; Huang, X., 2021. Measurement report:
560 Online measurement of gas-phase nitrated phenols utilizing a CI-LToF-MS: primary sources
561 and secondary formation. Atmos. Chem. Phys. 21(10), 7917-7932.
562 Sun, J.; Shen, Z. X.; Zhang, T.; Kong, S. F.; Zhang, H. A.; Zhang, Q.; Niu, X. Y.; Huang, S. S.; Xu,
563 H. M.; Ho, K. F.; Cao, J. J., 2022. A comprehensive evaluation of $PM_{2.5}$-bound PAHs and their
564 derivative in winter from six megacities in China: Insight the source-dependent health risk and
565 secondary reactions. Environ. Int. 165.
566 Teich, M.; van Pinxteren, D.; Wang, M.; Kecorius, S.; Wang, Z. B.; Muller, T.; Mocnik, G.;
567 Herrmann, H., 2017. Contributions of nitrated aromatic compounds to the light absorption of
568 water-soluble and particulate brown carbon in different atmospheric environments in Germany
569 and China. Atmos. Chem. Phys. 17(3), 1653-1672.
570 Vanni, A.; Pellegrino, V.; Gamberini, R.; Calabria, A., 2001. An evidence for nitrophenols
571 contamination in Antarctic fresh-water and snow. Simultaneous determination of nitrophenols
572 and nitroarenes at ng/L levels. International Journal Of Environmental Analytical Chemistry.
573 79(4), 349-365.
574 Vidovic, K.; Kroflic, A.; Jovanovic, P.; Sala, M.; Grgic, I., 2019. Electrochemistry as a tool for
575 studies of complex reaction mechanisms: The case of the atmospheric aqueous-phase aging of
576 aatechols. Environmental Science & Technology. 53(19), 11195-11203.
577 Vione, D.; Maurino, V.; Minero, C.; Borghesi, D.; Lucchiari, M.; Pelizzetti, E., 2003. New processes
578 in the environmental chemistry of nitrite. 2. The role of hydrogen peroxide. Environmental
579 Science & Technology. 37(20), 4635-4641.
580 Vione, D.; Maurino, V.; Minero, C.; Lucchiari, M.; Pelizzetti, E., 2004. Nitration and hydroxylation
581 of benzene in the presence of nitrite/nitrous acid in aqueous solution. Chemosphere. 56(11),
582 1049-1059.
583 Vione, D.; Maurino, V.; Minero, C.; Pelizzetti, E., 2001, Phenol photonitration upon UV irradiation

of nitrite in aqueous solution I: Effects of oxygen and 2-propanol. Chemosphere. 45(6-7), 893-902.

Wang, L. W.; Wang, X. F.; Gu, R. R.; Wang, H.; Yao, L.; Wen, L.; Zhu, F. P.; Wang, W. H.; Xue, L. K.; Yang, L. X.; Lu, K. D.; Chen, J. M.; Wang, T.; Zhang, Y. H.; Wang, W. X., 2018. Observations of fine particulate nitrated phenols in four sites in northern China: concentrations, source apportionment, and secondary formation. Atmos. Chem. Phys. 18(6), 4349-4359.

Wang, S. X.; Li, H., 2021. NO_3 center dot-initiated Gas-phase formation of nitrated phenolic compounds in polluted atmosphere. Environmental Science & Technology. 55(5), 2899-2907.

Wang, X.; Gu, R.; Wang, L.; Xu, W.; Zhang, Y.; Chen, B.; Li, W.; Xue, L.; Chen, J.; Wang, W., 2017. Emissions of fine particulate nitrated phenols from the burning of five common types of biomass. Environ. Pollut. 230, 405-412.

Wang, Y. J.; Hu, M.; Wang, Y. C.; Zheng, J.; Shang, D. J.; Yang, Y. D.; Liu, Y.; Li, X.; Tang, R. Z.; Zhu, W. F.; Du, Z. F.; Wu, Y. S.; Guo, S.; Wu, Z. J.; Lou, S. R.; Hallquist, M.; Yu, J. Z., 2019. The formation of nitro-aromatic compounds under high NO_x and anthropogenic VOC conditions in urban Beijing, China. Atmos. Chem. Phys. 19(11), 7649-7665.

Xie, M.; Chen, X.; Hays, M. D.; Lewandowski, M.; Offenberg, J.; Kleindienst, T. E.; Holder, A. L., 2019. Composition and light absorption of N-containing aromatic compounds in organic aerosols from laboratory biomass burning. Atmos. Chem. Phys. 19(5), 2899-2915.

Xie, M.; Chen, X.; Hays, M. D.; Lewandowski, M.; Offenberg, J.; Kleindienst, T. E.; Holder, A. L., 2017. Light absorption of secondary organic aerosol: Composition and contribution of nitroaromatic compounds. Environmental Science & Technology. 51(20), 11607-11616.

Yan, J. P.; Wang, X. P.; Gao, S. P.; Gong, P.; Dotel, J.; Pokhrel, B., 2023. Diagnostic ratio of nitrated phenols as a new method for the identification of pollution emission sources. Environ. Pollut. 316.

Yang, J. W.; Au, W. C.; Law, H.; Lam, C. H.; Nah, T., 2021. Formation and evolution of brown carbon during aqueous-phase nitrate-mediated photooxidation of guaiacol and 5-nitroguaiacol. Atmos. Environ. 254.

Yang, Y.; Li, X. R.; Shen, R. R.; Liu, Z. R.; Ji, D. S.; Wang, Y. S., 2020. Seasonal variation and sources of derivatized phenols in atmospheric fine particulate matter in North China Plain. Journal Of Environmental Sciences. 89, 136-144.

Yang, Z.; Tsona, N. T.; George, C.; Du, L., 2022. Nitrogen-containing compounds enhance light absorption of aromatic-derived brown carbon. Environmental science & technology. 56(7), 4005-4016.

Yuan, W., Huang, R.J., Yang, L., Wang, T., Duan, J., Guo, J., Ni, H., Chen, Y., Chen, Q., Li, Y., Dusek, U., O'Dowd, C., Hoffmann, T., 2021. Measurement report: $PM_{2.5}$-bound nitrated aromatic compounds in Xi'an, Northwest China-seasonal variations and contributions to optical properties of brown carbon. Atmos. Chem. Phys. 21, 3685-3697.

Yuan, W., Huang, R.J., Shen, J.C., Wang, K., Yang, L., Wang, T., Gong, Y.Q., Cao, W.J., Guo, J., Ni, H.Y., Duan, J., Hoffmann, T., 2023. More water-soluble brown carbon after the residential "coal-to-gas" conversion measure in urban Beijing. Npj Climate And Atmospheric Science 6.

Zhang, L.; Guo, X. M.; Zhao, T. L.; Xu, X. D.; Zheng, X. B.; Li, Y. Q.; Luo, L.; Gui, K.; Zheng, Y.; Shu, Z. Z., 2022a. Effect of large topography on atmospheric environment in Sichuan Basin: A climate analysis based on changes in atmospheric visibility. Frontiers In Earth Science. 10.

Zhang, L.; Hu, B.; Liu, X. L.; Luo, Z. H.; Xing, R.; Li, Y. J.; Xiong, R.; Li, G.; Cheng, H. F.; Lu, Q.; Shen, G. F.; Tao, S., 2022b. Variabilities in primary N-containing aromatic compound emissions from residential solid fuel combustion and implications for source tracers. Environmental Science & Technology.

Zhang, T.; Shen, Z. X.; Huang, S. S.; Lei, Y. L.; Zeng, Y. L.; Sun, J.; Zhang, Q.; Ho, S. S. H.; Xu, H. M.; Cao, J. J., 2022c. Optical properties, molecular characterizations, and oxidative potentials of different polarity levels of water-soluble organic matters in winter $PM_{2.5}$ in six China's megacities. Sci. Total Environ. 853.

Zhao, S. P.; Yu, Y.; Yin, D. Y.; Qin, D. H.; He, J. J.; Dong, L. X., 2018. Spatial patterns and temporal variations of six criteria air pollutants during 2015 to 2017 in the city clusters of Sichuan Basin, China. Sci. Total Environ. 624, 540-557.

Figure captions

Figure 1. Daily concentrations levels and compositions of four subclasses of NACs in six megacities (Green shadows represent the heavy polluted days). Average proportions of the four subclasses to ΣNACs during winterime (b) and summertime (c).

Figure 2. Correlations between individual NAC species and other chemicals in six megacities between winter and summer.

Figure 3. The transformation pathways of major NACs in atmospheric aerosols.

Figure 4. ΣNACs contributions to absorption of BrC in the six megacities during wintertime (left) and summertime (right).

Figure 5. Seasonal contributions of four NACs subclasses to the total light absorption of NACs in the six Chinese megacities.

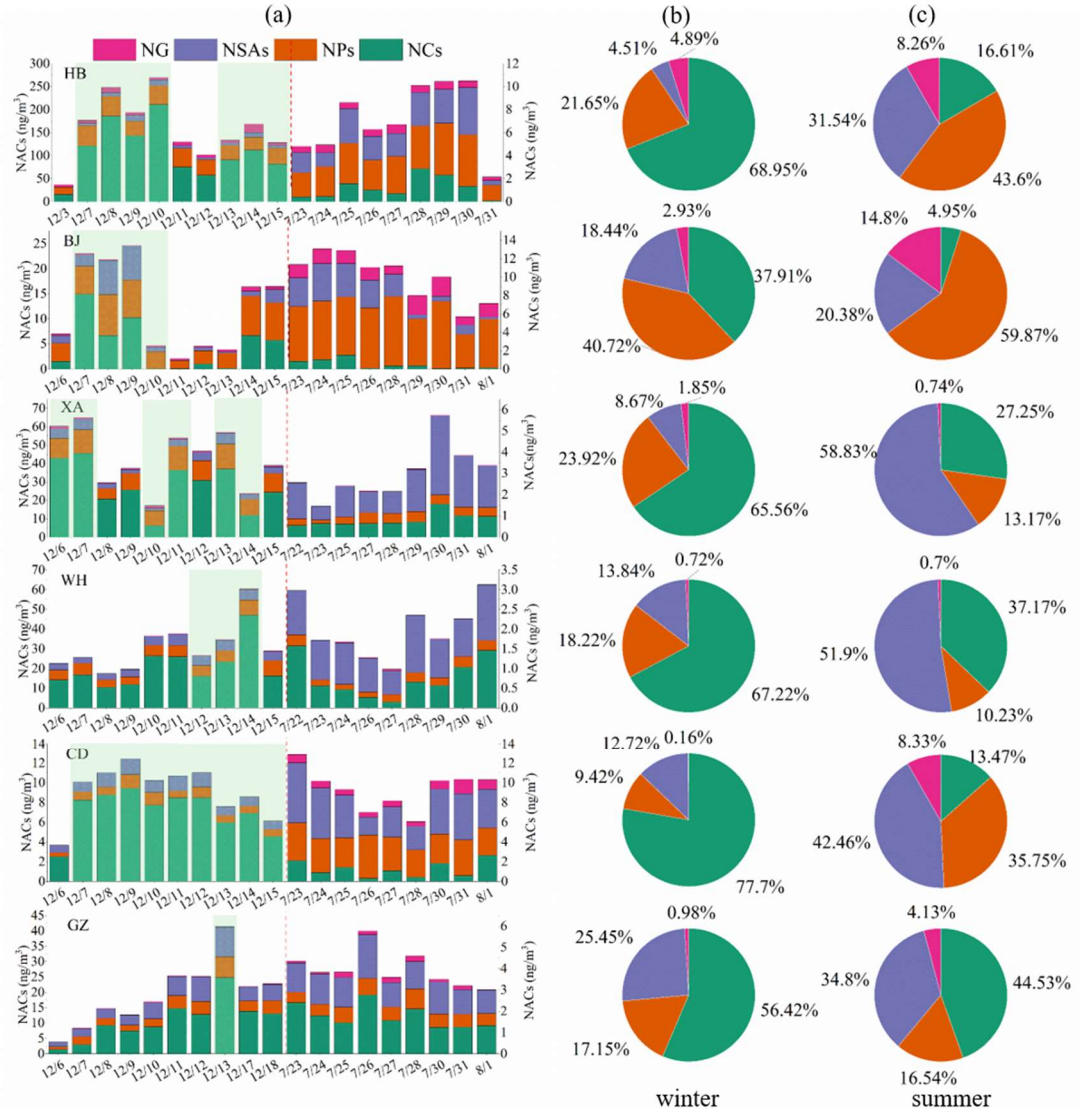

Figure 1. Daily concentrations levels and compositions of four subclasses of NACs in six megacities (Green shadows represent the heavy polluted days). Average proportions of the four subclasses to ΣNACs during winterime (b) and summertime (c).

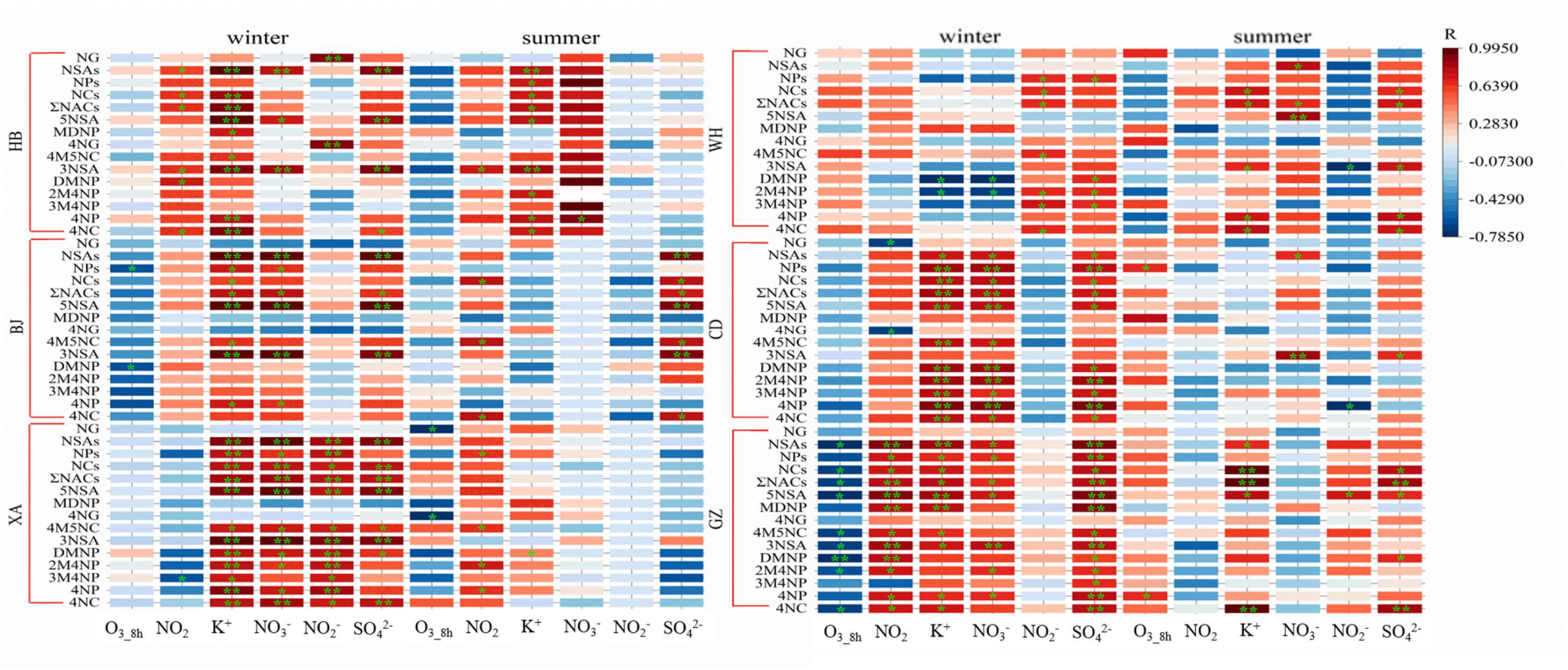

655

656 **Figure 2**. Correlations between individual NAC species and other chemicals in six megacities between winter and summer.

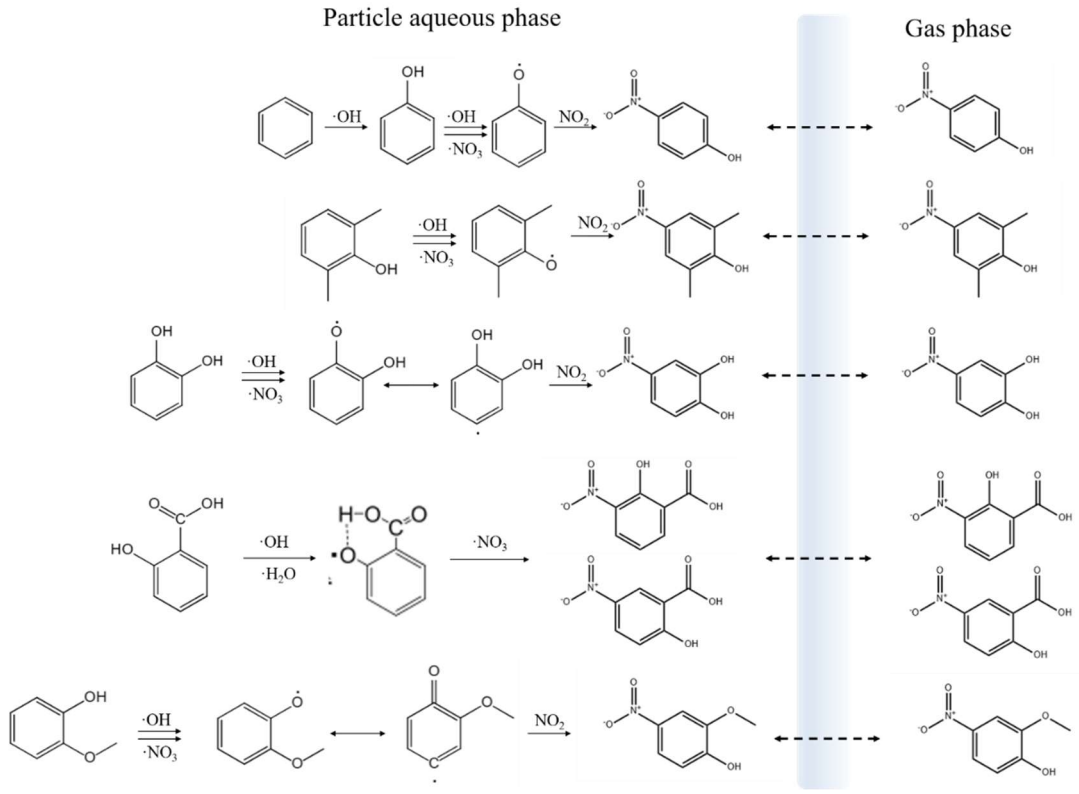

Figure 3. The transformation pathways of major NACs in atmospheric aerosols.

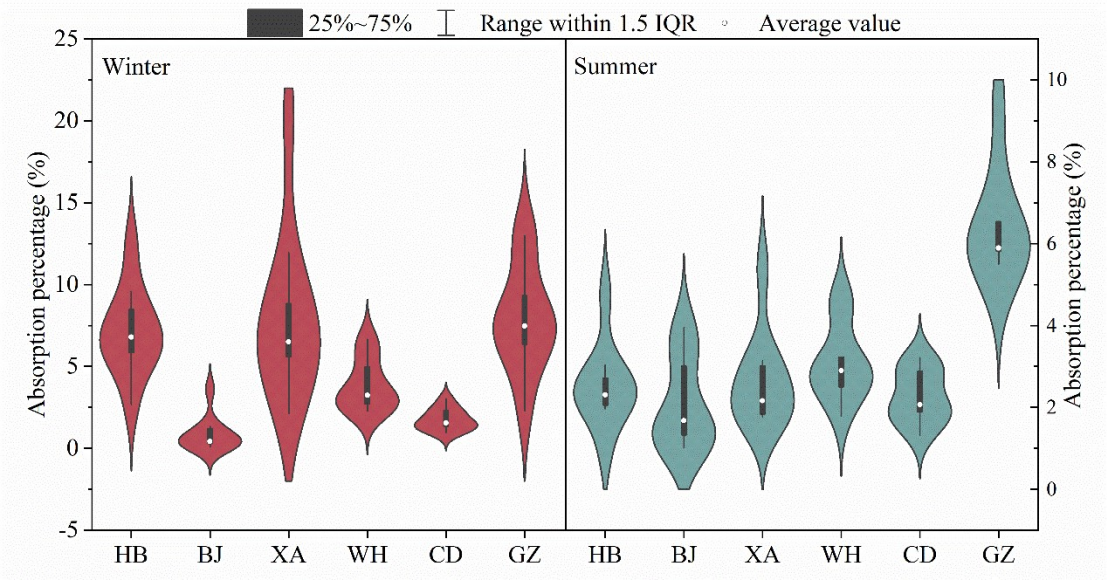

660

661 **Figure 4**. ΣNACs contributions to absorption of BrC in the six megacities during wintertime (left)

662 and summertime (right).

663

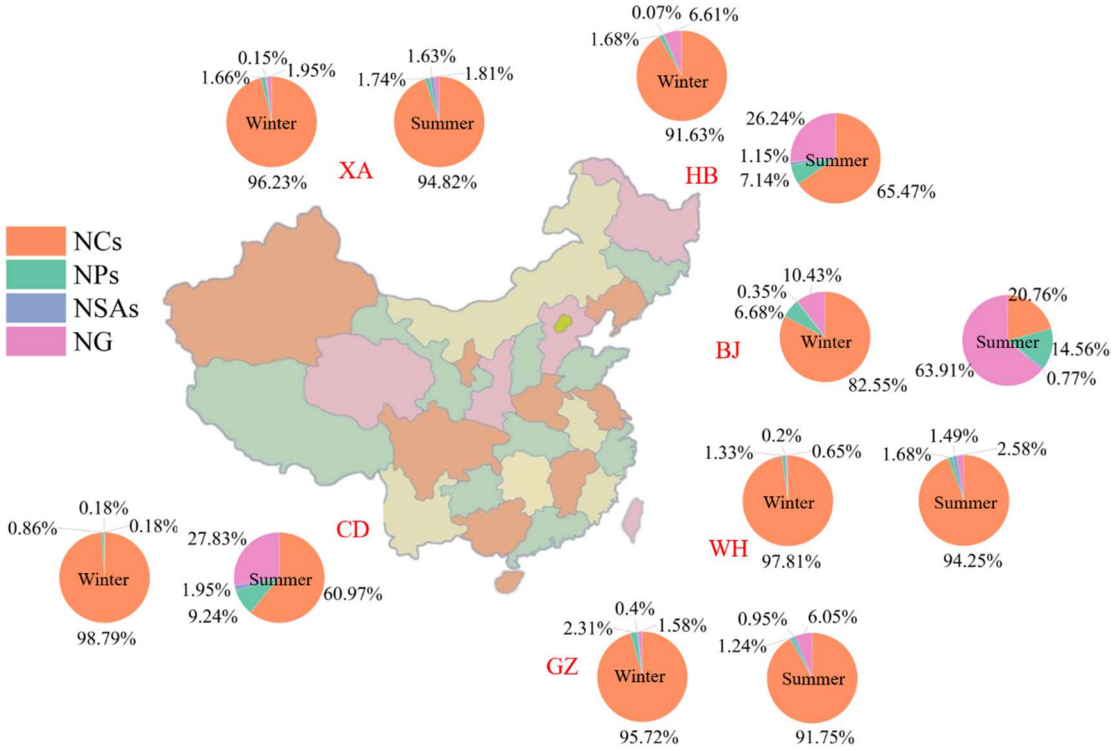

Figure 5. Seasonal contributions of four NACs subclasses to the total light absorption of NACs in the six Chinese megacities.

668 Table Captions

669 Table 1. Concentration levels of individual and total quantified NAC (ΣNACs) and
670 fraction in $PM_{2.5}$ in six megacities during the two seasons.

671 **Table 1**. Concentration levels of individual and total quantified NAC (ΣNACs) and fraction in $PM_{2.5}$ in six megacities during the two seasons.

City	Season	4NC	4NP	3M4NP	2M4NP	DMNP	3NSA	4M5NC	4NG	MDNP	5NSA	ΣNACs	ΣNACs/$PM_{2.5}$
		ng/m^3	ng/m^3	ng/m^3	ng/m^3	ng/m^3	ng/m^3	ng/m^3	ng/m^3	ng/m^3	ng/m^3	ng/m^3	‰
HB	Winter	94.51±50.36	6.02±1.54	9.37±2.36	16.83±4.50	0.52±0.15	2.79±1.55	14.97±9.23	7.77±4.20	1.64±0.65	4.38±2.22	158.79±68.63	1.78±0.43
	summer	1.07±0.84	1.09±0.47	0.42±0.15	1.39±0.45	0.04±0.02	0.47±0.29	0.13±0.10	0.59±0.13	0.20±0.06	1.80±0.83	7.18±2.94	0.23±0.08
BJ	Winter	4.22±4.58	0.75±0.33	0.73±0.39	1.43±0.65	0.06±0.02	0.80±0.88	0.52±0.53	0.37±0.24	0.43±0.24	1.50±1.64	10.80±7.74	0.36±0.29
	summer	0.46±0.48	1.10±0.32	0.92±0.80	1.34±0.26	0.04±0.01	0.51±0.44	0.04±0.03	1.49±0.43	0.59±0.25	1.54±1.06	8.02±2.15	0.64±0.30
XA	Winter	23.19±10.66	3.15±0.84	1.95±0.53	4.30±1.14	0.06±0.02	1.30±0.73	4.98±2.27	0.80±0.36	0.82±0.24	2.42±0.90	42.97±16.26	0.62±0.34
	summer	0.72±0.30	0.18±0.04	0.03±0.01	0.15±0.04	0.003±0.001	0.31±0.13	0.10±0.03	0.02±0.01	0.04±0.01	1.45±0.86	3.00±1.26	0.09±0.02
WH	Winter	17.77±8.66	1.56±0.28	0.79±0.28	2.55±0.91	0.05±0.02	1.26±0.47	3.09±2.13	0.22±0.12	0.71±0.27	3.04±0.68	31.04±12.43	0.40±0.13
	summer	0.67±0.45	0.09±0.02	0.01±0.00	0.09±0.03	0.002±0.001	0.26±0.10	0.08±0.07	0.01±0.01	0.02±0.01	0.79±0.18	2.02±0.73	0.09±0.03
CD	Winter	5.86±1.81	0.22±0.07	0.13±0.06	0.35±0.14	0.01±0.00	0.35±0.13	1.26±0.41	0.01±0.01	0.16±0.05	0.81±0.20	9.15±2.67	0.09±0.02
	summer	1.15±0.74	0.89±0.09	0.55±0.14	1.52±0.37	0.06±0.01	0.86±0.45	0.11±0.07	0.78±0.31	0.34±0.08	3.12±0.99	9.39±2.04	0.25±0.04
GZ	Winter	9.29±5.67	0.73±0.38	0.37±0.14	1.56±0.83	0.02±0.01	1.05±0.58	1.63±0.96	0.19±0.08	0.64±0.37	3.87±1.96	19.35±10.58	0.38±0.11
	summer	1.60±0.51	0.32±0.07	0.04±0.01	0.24±0.05	0.01±0.00	0.47±0.17	0.17±0.05	0.16±0.09	0.05±0.02	0.91±0.18	3.97±0.84	0.15±0.02

672